# Cause and Process Mechanism of Rockslide Triggered Flood Event in Rishiganga and Dhauliganga River Valleys, Chamoli, Uttarakhand, India Using Satellite Remote Sensing and in situ Observations

Pratima Pandey[1] · Prakash Chauhan[1] · C. M. Bhatt[1] · Praveen K Thakur[1] · Suresh Kannaujia[1] ·
Pankaj R. Dhote[1] · Arijit Roy[1] · Santosh Kumar[2] · Sumer Chopra[2] · Ashutosh Bhardwaj[1] ·
S. P. Aggrawal[1]

## Abstract

The catchments of Rishiganga and then Dhauliganga valleys in the Chamoli district of Uttarakhand were impacted by a catastrophic flood triggered due to a massive rockslide, caused by wedge failure on 7th February, 2021. It is estimated that the massive rockslide of $\sim$ 23 million cubic meter volume containing base rock, deposited ice, and snow got detached from the northern slopes of the Trishul mountain range near Ronti Glacier and created a vertical fall of almost 1700 m before severely impacting the Ronti Gad valley located at 1.5 km downstream of Ronti Glacier snout. The huge detached mass of rock and ice (GLIMS ID: G079733E30381N) swiftly moved downstream through the glaciated valley entraining snow, debris, mud on its way, caused rapid fluidization, created massive water/slush waves, and washed away partially or completely the hydel power projects and bridges in its route. It is estimated that $\sim$ 0.93 Peta Joules of potential energy led to the generation of a significant amount of kinetic and thermal energy, good enough to trigger above-mentioned processes. Post-event analysis of high-resolution satellite data shows flood water marks in the valley and on the rock outcrops reaching up to $\sim$ 80–150 m height on the way to Raini Village. The mud and the slush produced through this process led to the formation of a dammed lake and temporarily blocked one of the tributaries of the Rishiganga joining from the northeast. This study provides an insight into the sequence of events as they unfolded, through multi-temporal satellite image analysis, aerial survey, seismological data in conjunction with various other geo-spatial and geo-visualization tools for unraveling the flood event that has happened on February 7, 2021. We also discuss the potential cause of rockslide and the process mechanism of this unique event, causing loss of lives and property besides widespread devastation.

**Keywords** Rockslide · Flood · Himalaya · Remote sensing · Chamoli Uttarakhand

## Introduction

The global climate change and global warming trends are unmistakable from the long-term atmospheric, terrestrial, and oceanic data. With the increase in the global warming, the frequency of extreme events is also expected to increase (Hoegh-Guldberg, 2018, IPCC), especially in the mountainous regions. The Himalayan region is experiencing a significant rise in temperature over the last few decades, more than the global average, especially the winter temperature (Bhutiyani et al., 2010; Negi et al., 2018; Shreshtha et al., 1999 and references therein). With the result, the Himalayan cryosphere experiences enhanced melting and have led to the formation/expansion of glacial lakes, permafrost thaw, and snow/ice/debris avalanches (Dobhal et al., 2013; Champati Ray et al. 2015; Kumar, 2019; Pandey et al., 2020, 2021 and references therein). Eventually, the natural hazards in high mountain areas associated with the glacial environment, such as ice/rock avalanches, rockslide, landslides, debris flows, and glacial lake outburst

✉ Prakash Chauhan
prakash@iirs.gov.in

1 Indian Institute of Remote Sensing, ISRO, 4, Kalidas Road, Dehradun, India

2 Institute of Seismological Research, Gandhinagar, India

floods (GLOFs), have also increased and resulted in the extensive loss of lives and property (Carrivick & Tweed, 2016; Deshmukh et al 2011; Gruber & Haeberli, 2007 and references therein). In high mountain regions like the Himalaya, climatic variation may reduce the strength and cohesiveness of rocks along with critical geological setup and can always facilitate slope instability due to reducing rock strength (Fischer et al., 2012). Similarly, the glacier-permafrost linkage processes will also influence the stability of the steep hanging ice bodies and the rock walls, which are continually weakened under the recurring warming and freezing. However, the complex interactive mechanism is yet to be fully understood (Fischer et al., 2012). The increasing risk by natural disasters in the Himalayan region necessitates employing advanced technologies in monitoring, as well as to study the cause and effects of natural disasters in the region. This is also in accordance with one of the priorities of action of the Sendai framework, which identifies "Understanding Disaster Risk." The recent catastrophic flood experienced on February 7, 2021 in the catchment of Rishiganga and Dhauliganga valleys in the Chamoli district of one of the Indian Himalayan state, Uttarakhand, has yet again impelled scientists worldwide to recognize the fragility of the rocks, glacial system, and environment in the Himalayan terrain under the prevailing climate change scenario. In the present study, we combined satellite data and aerial survey to bring out the possible mechanism and to unfold the sequence of events as occurred on the morning of February 7, 2021.

## Study Area

Located in the Central Himalaya, Rishiganga valley occupies a transitional zone between the moist Indian Summer Monsoons (ISM) dominated Himalaya (south) and the cold and dry highlands of Tibet. These young mountains are structurally very fragile and are exposed to the extreme climatic conditions prevalent in the region. The tropical character of the region with high biodiversity and spectacular mountain landscapes is in a large consequence of topography-climate interactions. The area is predominantly influenced by the ISM, however, the mid-latitude westerlies also contribute to the snowfall in the winter that feeds numerous glaciers in the region. These weather systems control the cryosphere, landscape dynamics, ecosystems and socioeconomic fabric of the inhabitants in this region. The topography of the regions is very rugged with steep slopes with elevation varying between 3000 and 6000 m from the mean sea level. Topographically, the region comprises of high peaks separated by narrow valleys and deep gorges. The study area forms part of the Alaknanda Catchment and is crisscrossed by several important rivers and associated tributaries, which are fed by melt waters of high-altitude snow-covered peaks and glaciers. Geologically, the study area is bounded by Vaikrata Thrust to the south and Malari Fault on the North and belongs to the Vaikrata Group of high-grade metamorphic rocks (kyanite gneiss, staurolite, quartzite, garnet, and biotite schists) that have been intruded by both acidic and basic rocks. The litho units are highly jointed and fractures as well. Figure 1 shows the overview and topographic
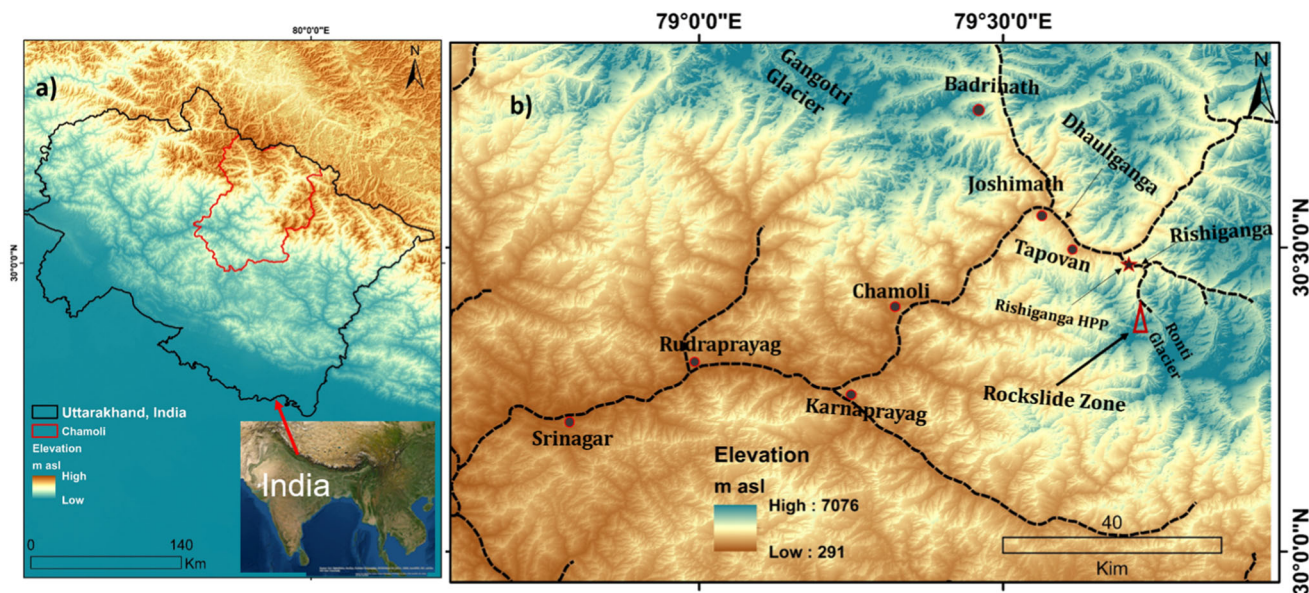


Fig. 1 Overview of the location of the flood impacted Rishiganga and Dhauliganga valley as shown using ALOS DEM (12.5 m spatial resolution) freely available from Alaska Satellite Facility. The Inset India map in (a) has been obtained from the basemap, ArcGIS 10.1. The HPP in (b) stands for Hydropower Project

variability of the area under investigation for this flood event of February 7, 2021.

## Datasets Used

Availability of timely data, both satellite-based earth observation data, as well as *in situ* observations, during a disaster is very crucial to understand the overall dynamics of the event for taking decisions and actions by the authorities (Bhatt et. al., 2017; Martha & Kumar, 2013). During a catastrophy over high altitude regions like the Himalaya, the role of International Charter Space and Major Disasters (ICSMD) for the continuous and quick response due to combined space assets from multiple space agencies becomes very valuable. Since this disaster in Chamoli has occurred at an altitude of about 5600 m and the entire valley was in spate largely with mud and debris flow deposits, the area remained inaccessible. Identifying the exact location, the spatial extent of the disaster, and the cause that actually triggered the event was not feasible using conventional means. For this particular event, ICSMD was triggered (Call-803) by the Indian Space Research Organisation (ISRO) on February 7, 2021 and the Indian Remote Sensing (IRS) Satellites were also tasked on priority over the affected valley. This particular event presents a classic example where the multi-temporal satellite images played a critical role in visualizing and deciphering the sequence of events leading to the disaster. This study could also bring a closure on lingering confusion on the probable cause and process mechanism of this event.

Pre- and post-disaster high-resolution satellite images used in this study are presented in Table 1. In addition to the satellite images, digital elevation model from Indian Cartosat-1 satellite (10 m spatial resolution), ALOS DEM (12.m spatial resolution), and TandDEM-X (30 m spatial resolution) are also used for hydrological simulations and 3D view generation for understanding the topography of the area. The Pleiades panchromatic (PAN) and multi-spectral (MS) stereo satellite datasets were used to generate DEMs for computing the thickness of the broken rock and ice mass. The stereo datasets were processed for satellite triangulation using rational polynomial coefficients (RPCs) in photogrammetric environment yielding RMSE of 0.15 pixels and 0.05 pixels for PAN and MX stereo datasets, respectively. DEMs were generated at 0.5 m and 2.0 m from stereo PAN and multispectral datasets, respectively. The DEMs and orthoimages were found highly useful for visualization and analysis. Satellite-based observations are supported by observations from the aerial survey, carried out over the affected valley four days after the event, i.e., on February 12, 2021, through the support of the Uttarakhand State Disaster Management Agency (USDMA) and Indian Air Force (IAF).

## Observations

### Satellite-Based Observation of the Event and cause of Flood Water Production

In the morning of February 7, 2021 at around 1100 h Indian Standard time (IST), the news of a massive flood in Rishiganga and Dhauliganga rivers causing large-scale destruction to the infrastructure, especially hydropower stations, bridges and roads as well loss of human lives started streaming the social media and television networks.

**Table 1** Satellite data used for the analysis

| Acquisition date | Satellite | Sensor | Resolution |
| --- | --- | --- | --- |
| *Pre-event* | | | |
| 18/10/2020 | IRS LISS IV | MX | 5.8 m |
| 31/01/2021 | IRS Resourcesat-2 | LISS IV MX | 5.8 m |
| 31/01/2021 | PlanetScope | MX | 3.0 m |
| 03/02/2021 | IRS LISS IV | MX | 5.8 m |
| 05/02/2021 | Sentinel-2 | MSI | 10 m |
| 05/02/2021 | PlanetScope | MX | 3.0 m |
| *Post-event* | | | |
| 07/02/2021 | PlanetScope | MX | 3.0 m |
| 07/02/2021 | PlanetScope | MX | 3.0 m |
| 08/02/2021 | IRS Cartosat-2A | PAN | 0.8 m |
| 08/02/2021 | IRS Resourcesat-2 | LISS III | 24 m |
| 08/02/2021 | IRS Resourcesat-2 | LISS IV MX | 5.8 m |
| 09/02/2021 | Pleaides | PHR-1A MS | 2.0 m |
| 10/02/2021 | Pleaides | PHR-1B PAN & MS | 0.5 m &2.0 m |

**Fig. 2 a** 3D perspective of the event explained on IRS LISS IV image draped on Cartosat DEM; **b** PlanetScope data of February 7, 2021 at 10.35hrs IST capturing the dust plume generated due to the event
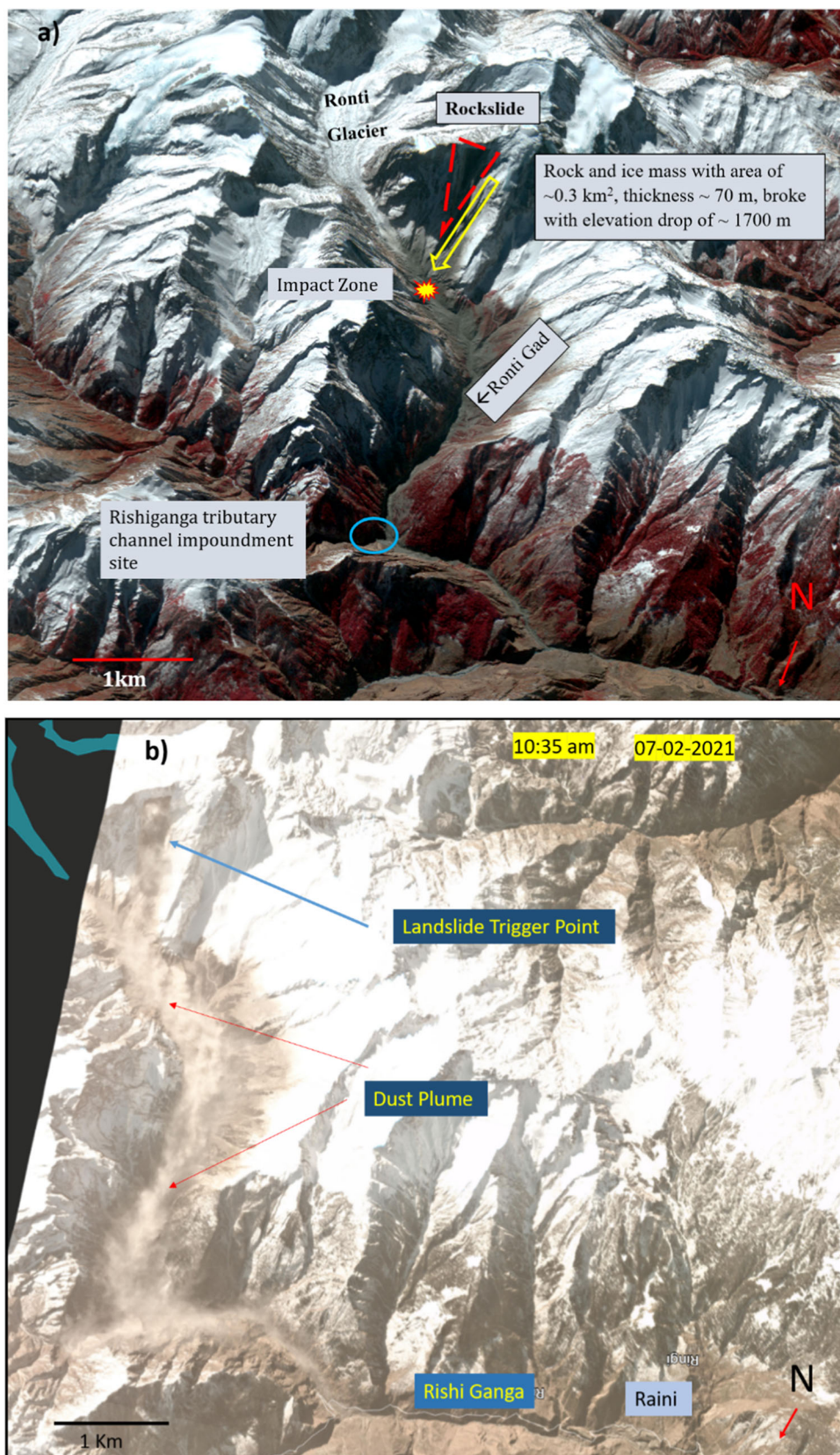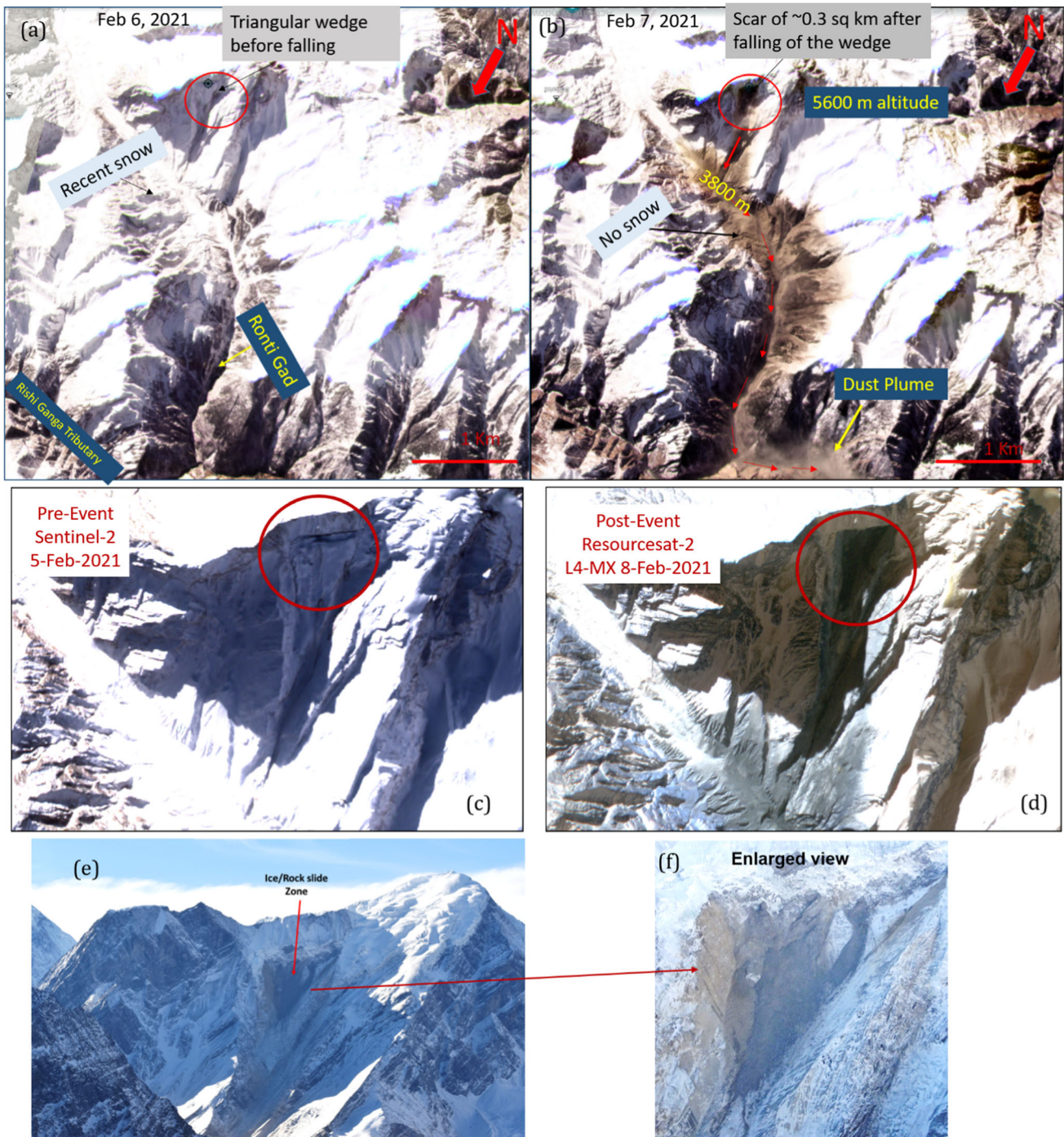
**Fig. 3** PlanetScope images of **a** February 6, 2021 showing freshly fallen snow; and **b** February 7, 2021 showing the snow covered by dust after the rockslide. The plume of dust in the valley is also visible in the image; **c** Sentinel-2 image of February 5, 2021 pre-rockslide; **d** IRS Resourcesst-2 LISS IV MX image on February 8, 2021 showing post-rockslide and **e–f**) Photographs of the rockslide event as observed through aerial survey on 12 February 2021 view is to the southeast

Initially, the media reports suggested GLOF as the cause behind this event. The abnormal rise in the water level to ∼ 16 m at Joshimath was observed by India's Centre Water Commission (CWC). However, initial satellite observations over the region ruled out any GLOF event as there were no indications of any lake existed in the region. On the other hand, various satellite data analyzed indicated the signature of a large chunk of rock that has detached from the ridge adjoining the Ronti Glacier, which feeds the Rishiganga river, eventually led to the subsequent events of
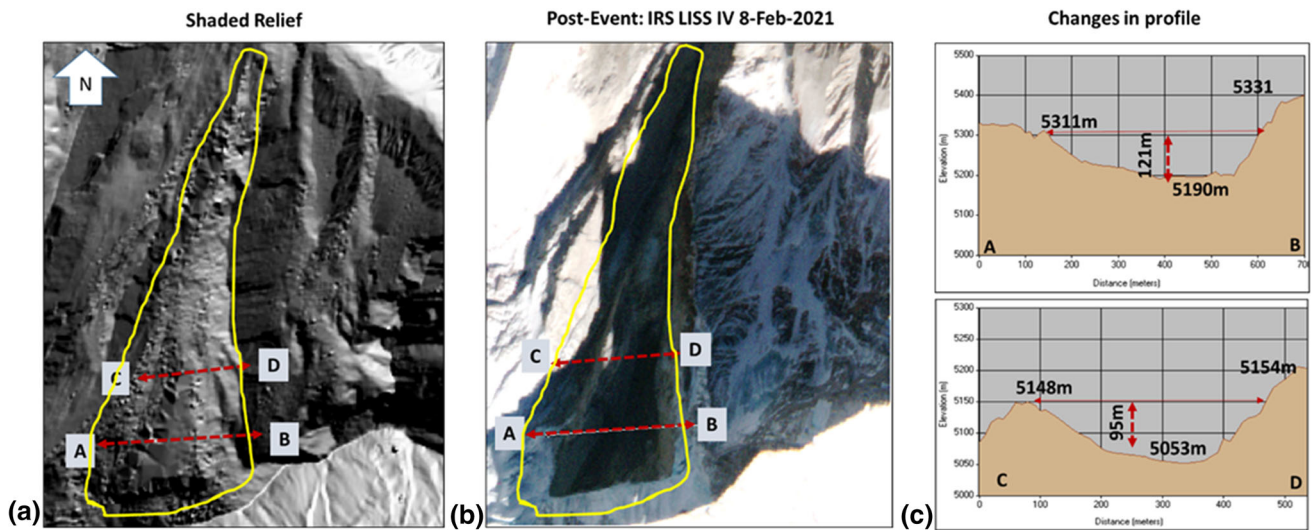
**Fig. 4** Relative change on the DEM profile of the scar region post-rockslide. **a** Shaded relief, **b** IRS LISS IV post-rockslide image, **c** profile along sections A-B and C-D between undeformed and deformed part (central). An average value of 70 m DEM difference is considered for the entire scar region to calculate the volume of the detached mass
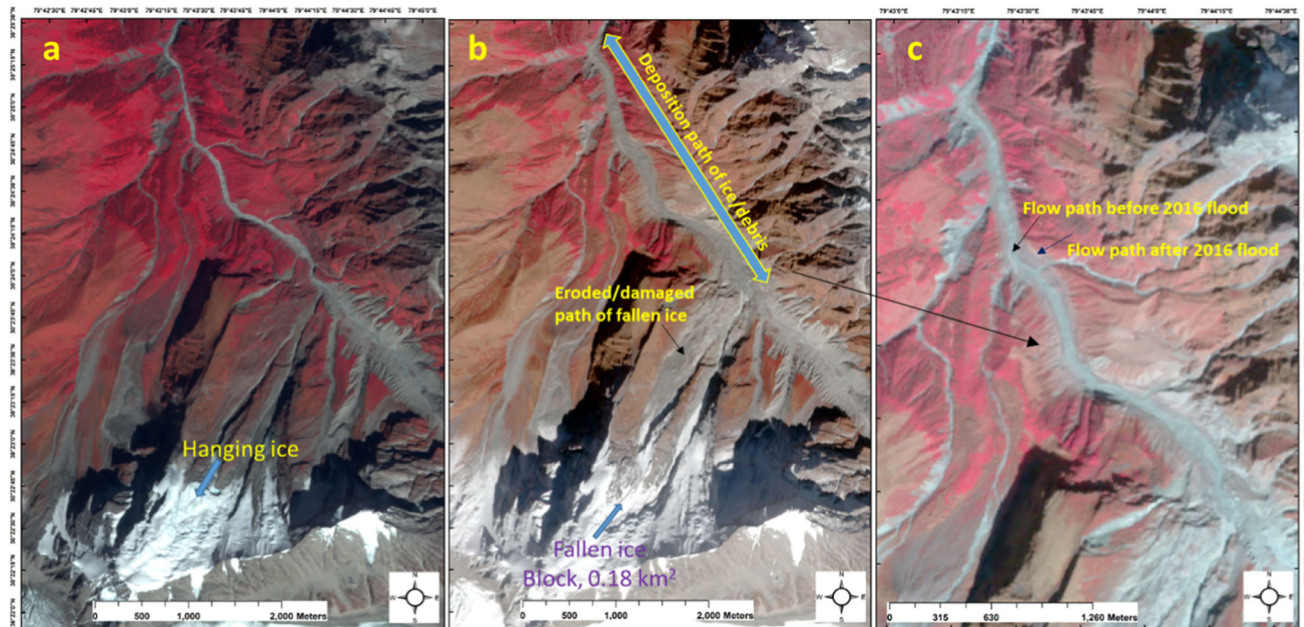


**Fig. 5** Remote sensing (Sentinel-2 MSI data)-based sequence of events for 2016 icefall. **a** 19 September 2016 image showing intact hanging ice; **b** 09 October 2016 image showing broken part of hanging ice and **c** icefall-induced mixed debris flow and deposited material seen in 09 Oct 2016 image (shown with 20% transparency)

extensive destruction and damage (Fig. 2a). The Planet Labs satellite images acquired on February 07, 2021 at around 1035 h (IST) also showed an extensive plume of dust generated traveling downstream in the valley from the impact zone (Fig. 2b). The Planet Labs data proved that the event was ongoing at the time of satellite pass at the region.

Analyses of pre- and post-satellite images (Fig. 3) from various sources show the sequence of the slide in the valley. A huge chunk of hanging snow- and ice-covered rock mass (located at 30°22′39.62"N, 79°43′57.52"E, ∼ 5600 m asl, GLIMS ID: G079733E30381N), on the northern slopes of Trishul mountain (Fig. 3a), locally known as "Ronti" (∼ 1.5 km downstream of Ronti Glacier) has broken off and triggered the entire disaster. Figure 3 b–e shows the rockslide triggered zone, after the event as seen on the satellite image and by our dedicated aerial survey carried out in the area. The north-facing hanging rock and ice mass had a mean slope of ∼ 39° and was situated at a

median altitude of ∼ 5600 masl, i.e., ∼ 1700 m above the valley floor. The rock mass that broke off was estimated to occupy an area of ∼ 0.34 km$^2$, with a mean length 850 m and width of 550 m show a triangular wedge failure shape (Fig. 3d-f). Based on the aerial observations carried out by hovering very closely to the slide location and post-event analysis of DEM, the average thickness of the detached and dislodged mass was estimated to be ∼ 70 m. The profiles between the deformed and undeformed adjacent surfaces based on the post event DEM are shown in Fig. 4. Considering breaking off of a volume of ∼ 23 million cubic meters from a fall height of ∼ 1700 m, potential energy of ∼ 0.93 Peta Joules has been calculated (considering 80% rock and 20% ice). The sliding process eventually transferred the potential energy into an enormous amount of kinetic energy and thermal energy, triggering mobilization of water-saturated sediments (entrained ice, snow, debris and boulders) through fluidization, which was considered to be responsible for creating the devastating flood in the Rishiganga and Dhauliganga valleys.

Signature of a similar, however, of lesser magnitude flood event has been deciphered through time series analysis of satellite images (Fig. 5). Based on the evidence from analyses of Sentinel-2 images, the flood might have occurred between September and October 2016 which had deposited ice/mud/debris along 3.6 km downstream the Ronti Gad from the presently impacted zone (Fig. 5).

The rockslide that occurred on February 7, 2021 immediately triggered a dust plume as seen from the post-event images. Analyses of the pre- and post-satellite images from IRS LISS IV sensor also show huge volume of sediments deposited all along the river valley, especially between Raini village and Joshimath. The mean river valley width changed from 20 to 40 m during the pre-flood period, to 115–532 m during post-flood time, as per the analysis made on IRS LISS-IV images. The high-water level marks all along the valley and the loss of vegetation due to the event are clearly discernible on satellite images (Fig. 6a-b). The increase in the flow velocity and carrying capacity of the river has brought noticeable changes in the channel width and fluvial deposits in downstream. The maximum change in the valley width is observed at the confluence of Ronti Gad and Rishiganga rivers, where the width has increased to 532 m. As compared to the left bank with deposits stretching 100 m, more deposition is observed on the right bank side. This is mainly due to sudden change in fluvial process with a rapid deflection in the flow direction from North to Northwest, and energy redistribution of fluid flow due to high discharge. The rolling
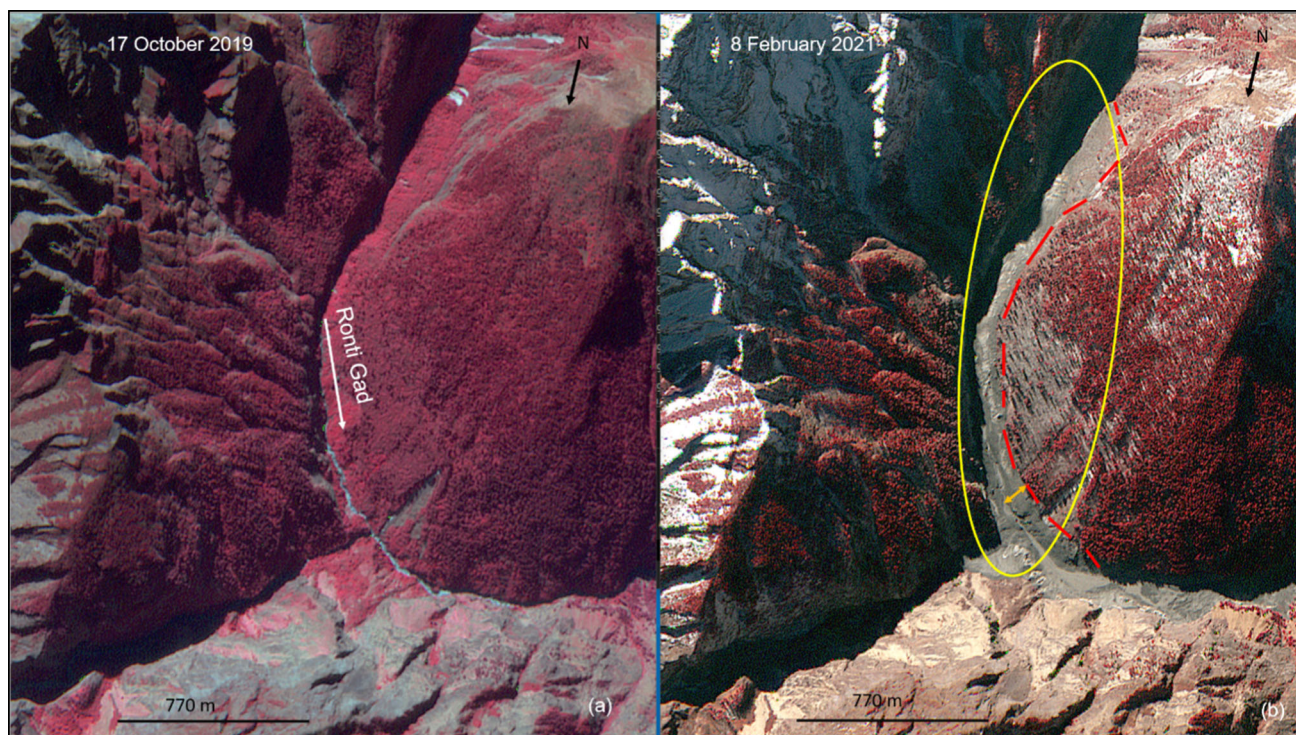


**Fig. 6 a–b** IRS LISS-IV MX data (draped over Cartosat DEM) for pre (dated October 17, 2019)- and post (dated February 8, 2021)-event showing changes in the river valley due to the flood. The dotted lines (in red) and the arrow (in yellow) marked in the figure **b** show increase in valley width due to strong fluvial activity in the Ronti Gad

**Fig. 7** Aerial photograph (looking toward northeast) of the breaching of the river impoundment (Rishiganga tributary) due to the rockslide in Rishiganga upper catchment

debris material being carried away due to the steep gradient initially washed away the Rishiganga hydropower project and subsequently washed away the bridge (connecting Raini village), which was located at 1.45 km and 0.45 km upstream, respectively, at the confluence of the Rishiganga and the Dhauliganga rivers. The Tapovan hydropower project located ∼ 6 km downstream from the above confluence was then damaged. The debris also temporarily blocked the flow of one of the tributaries of the Rishiganga river located 430 m NE of its pre-flood confluence with Ronti stream (79 43 56.3 E; 30 27 59.42 N; ∼ Elevation 2337 m) and created a dammed lake (77 44 10.78 E; 30 28 5.45 N; Elevation ∼ 2410 m) with an aerial spread of 2.12 ha (as per observation on February 9, 2021) and 500 m in length. However, this lake has gradually breached through a small outlet across the unstable debris dam (Fig. 7); therefore, it seems to have not much potential for creating any future outburst flood as observed during the aerial survey carried out on February 12, 2021. However, the large amount of mud deposited around it can create future obstruction to the flow of Rishiganga river, especially during Monsoon period.

## Seismological Observation of the Event

The event has also been perceived from the seismological point of view by analyzing seismograms of four seismometers installed by the Indian Institute of Remote Sensing (IIRS), Dehradun at Mandal (∼ 75 km away from the event zone); Nainital (∼ 145 km); Kotdwar (∼ 185 km) and Mussoorie (∼ 210 km) stations. All four stations are found to have recorded a seismic activity (waves between 0451 and 0454 UTC, i.e., 10.21 h to 10.24 h IST, on February 7, 2021) around the same time as of the rockslide event (Fig. 8). The recordings of the seismometers revealed that the impact has generated seismic waves consisting of mainly surface waves, which could be recorded even at far off distances up to 210 km from the present impact site in the present case. However, all the seismograms clearly lacked body waves signatures. Absence of body waves clearly ruled out the occurrence of any earthquake in the region. The surface waves decay more slowly than the body waves and can travel far off distance from the point of origin. The speed of surface waves is around 0.9 times than the speed of the S-waves.
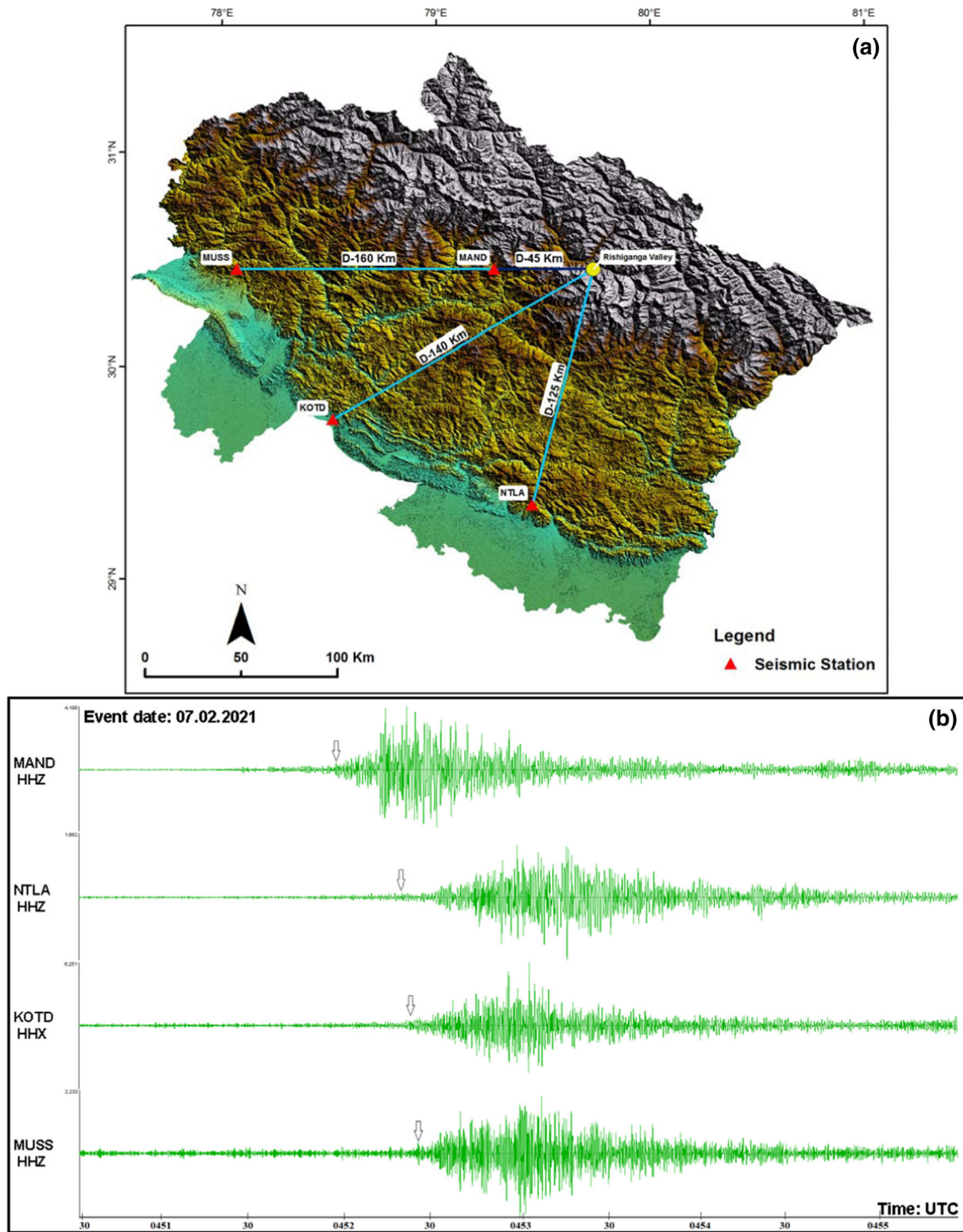
**Fig. 8 a** Map illustrating all the four seismic stations monitored and maintained by IIRS (MAND, NTLA, MUSS, and KOTD) selected for studying the Rishiganga valley event of February 7, 2021. **b** The waveform images of the four seismic stations showing recording of the surface wave. The arrow indicates the start of surface waves

By considering the speed of S-waves around $\sim 3.4$ km/s at the surface, the speed of surface waves will be around $\sim 3$ km/s. Accordingly, the waves may take around 25 s to reach Mandal site, around 50 s to reach Nainital, 60 s to Kotdwar, and 70 s to Mussoorie from the impact zone. We have compared the relative arrival times of the surface waves at all the recording sites (Table 2) and found that they all match well with the time of the

**Table 2** Arrival time of surface waves at different stations of IIRS

| Station | Aerial distance from impact site (km) | Arrival time of surface waves (IST) | | |
|---|---|---|---|---|
| | | Hr | Mn | Sec |
| Mandal | 75 | 10 | 22 | 0.19 |
| Nainital | 145 | 10 | 22 | 19.55 |
| Kotdwar | 185 | 10 | 22 | 23.71 |
| Mussoorie | 210 | 10 | 22 | 25.22 |

occurrence of the rockslide. Therefore, it is inferred that the massive rockslide was not triggered by an earthquake, contrarily it has generated seismic waves.

## Hydrodynamic Simulations of the Flood

The flood event initiated in the Rishiganga River valley on February 7, 2021 is an example of one of its kind that included mix flow of ice, snow, rock, debris, mud, and water. An attempt was made to simulate the complex flow using one-dimensional (1D) hydrodynamic (HD) model (MIKE 11) to assess the impact of the flood in the downstream locations namely Nandaprayag, Karnaprayag, Rudraprayag, and Srinagar in the Uttarakhand Himalaya.

The MIKE-11 model was chosen based on the suitability of HD models for narrow valley basins of Himalayan region such as Dhauliganga river (Thakur et al. 2016; Dhote et al. 2018 and 2019). The river network was digitized using Google Earth high-resolution image from flood source site to the Srinagar. The space-borne TanDEM-X-based Copernicus DEM (30 m) was used to extract cross sections without considering the bathymetry. The Manning's roughness coefficient ($n$) adopted for channel and floodplain was 0.028 and 0.08, respectively (Chow et al., 1988). Based on the social media videos, different flood inundation scenarios were assessed using initial approximate peak discharge varying from 3500 to 7500 cumec as inflow upstream boundary condition in HD model (Fig. 9a). The
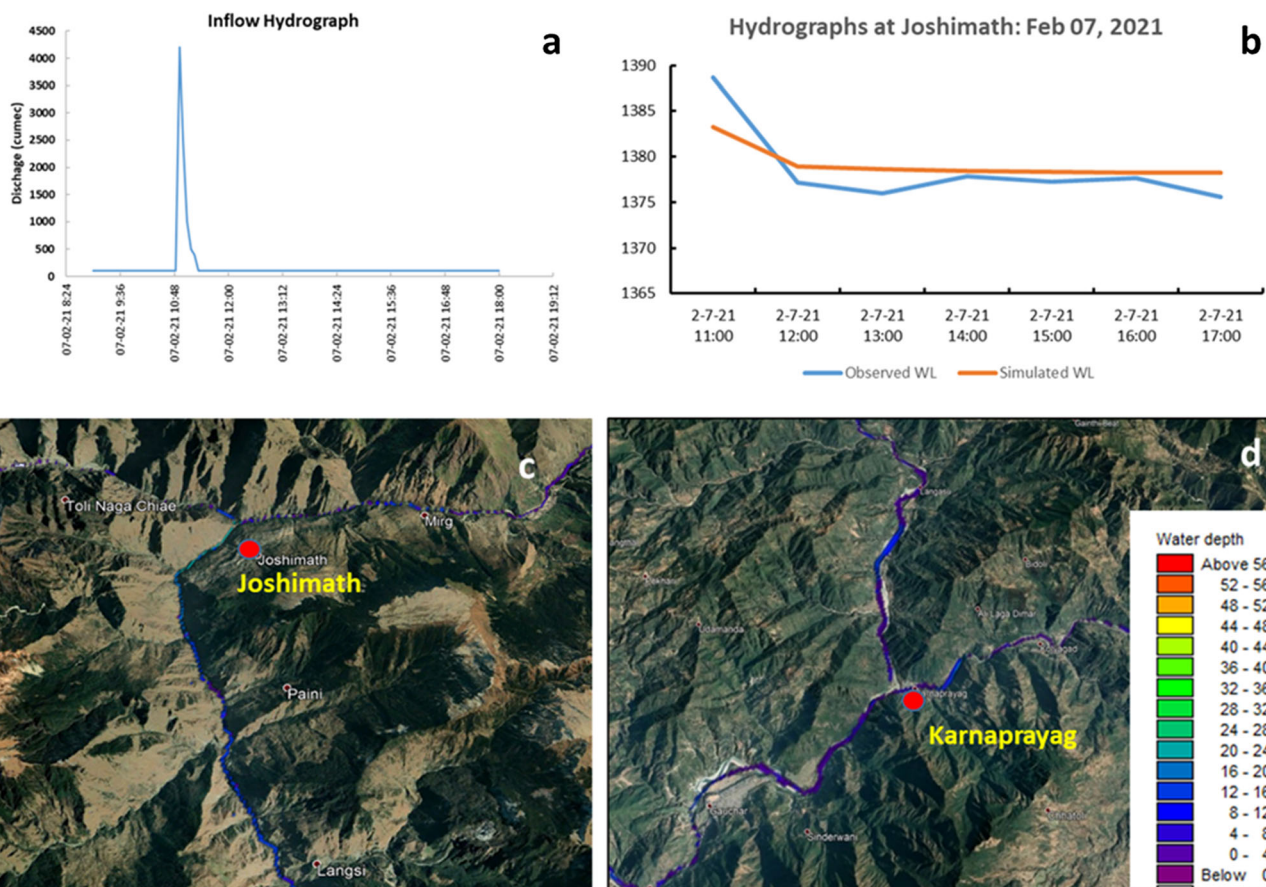


**Fig. 9** Hydrodynamic simulation of the flood event in Dhauliganga and Rishiganga on February 7, 2021: **a** inflow hydrograph at upstream boundary; **b** comparison of simulate and observed water level; (**c** & **d**) Flood extent and depth at Joshimath and Karnaprayag

minimum flow of 50 cumec was assumed as lateral flow for all the other tributaries. All the results discussed here are with respect to the 4200 cumec peak discharge scenario at source site in Ronti gad. The comparison of the simulated and the observed water level at Joshimath gauging site corresponding to 4200 cumec scenarios is shown in Fig. 9b. The flood depth was varying and started attenuating as we move from upstream to the downstream, i.e., 12–24 m from Raini village to Joshimath and 1–4 m at Karnaprayag and Rudraprayag (Fig. 9 c and d.). Since the river flow was drastically controlled by a barrage at the hydropower site at Srinagar, the impact was significantly reduced in the downstream areas. The time of travel for the peak flood wave from glacier site upto the Raini, Tapovan, and Joshimath is estimated to be as $\sim$ 05, $\sim$ 10, and $\sim$ 20 min, respectively, covering a distance of 14 km, 22 km, and 34 km, respectively. The velocity varied between 33.43 and 7.9 m/s, with a mean velocity of $\sim$ 15.85 m/s from the source site to Joshimath. It was confirmed by National Thermal Power Corporation Ltd. officials that water wave reached Tapovan at 1038 h. IST, also confirming these observations.

The present HD model simulations were carried out in near real time to reduce severe destruction to human lives and infrastructure using limited freely available data. The TanDEM-X DEM-based cross sections do not depict the bathymetry of the channel that may impact estimation of the conveyance of the channel. MIKE 11 solves Saint Venant equations (Dhote et al., 2019 and references therein) in fully dynamic mode which works adequately for riverine flooding due to extreme rainfall or glacial lake outburst. However, this model may not simulate such complex flow that exhibits huge quantity of ice and debris. The reasonable degree for uncertainties is associated with the model parameterization and computational constraints (e.g., time step), which results in considerable variation in outputs.

## Discussion and Assessment of the Mechanism of the Event

It was evident from the temporal analysis of the pre-event images available in the Google Earth and Planet labs data that the commencement of fracturing in the headwall of this rock and ice mass has started way back in 2017. The fracture processes within an ice body and stresses in the fracture zone are suggested to be the probable cause of the destabilization of a mass (Faillettaz et al., 2015) on steep slopes. The stresses in the fracture zone are further dependent on the topography of the hanging ice, slope steepness, weather conditions including temperature and precipitation, wind direction, and wind speed. The slopes in

the range of 30–40° are found to be the most prone for mass movement (Snehmani et al. 2014). The northern-facing Himalayan slopes remain in the shadow throughout the day during the winter. Further, heavy snowfall on the steep slope/side increases the vulnerability through over steepening and overloading. Furthermore, day-old snow is most unstable and has high potential to result in avalanche. The rock and ice body on the Ronti peak was situated on a steep slope ($\sim$ 39°) oriented toward the north. Keeping these facts in view and looking at the local weather data, it has been found that the area has received a good amount of snowfall during February 3 and 4, 2021 (Figs. 10a–b). A good accumulation of snow is also observed over the region from the comparison of Resourcesat-2 LISS IV MX data of January 31, 2021 (Fig. 10a), and Sentinel-2A of February 5, 2021 (Fig. 10c), which shows depletion in subsequent images acquired on the day of the event (Planet Lab data, Fig. 10b) and post-event (LISS IV, Fig. 10d) over the region. The time series analysis of an early run 0.1 deg of GPM data (GPM_3IMERGDE v06) daily accumulated precipitation (combined microwave-IR) estimate over the region showed high precipitation on February 3 and 4, 2021(Fig. 10e). The WRF model forecast, from MOSDAC (https://www.mosdac.gov.in/) also confirmed the rise in snow precipitation during February 4–6, 2021 in the Rishiganga and Dhauliganga valleys, which thereafter was observed to be reduced significantly. The weather was clear and sunny on February 6 and 7, 2021, and there was a sudden rise in the temperature felt by people in the nearby areas and also in congruence from WRF simulations (MOSDAC). An abrupt change in the weather conditions coupled with the climatic variations influencing glacier-permafrost regimes must have altered the thermal condition of the hanging rock and ice by influencing the bedrock stability.

Experimental and field studies have established that from an impacting mass, kinetic energy can be transformed into acoustic energy (shock waves) along with thermal energy (Huggel et al., 2005; Kieffer & Simonds, 1980). In the present case, the impact of the mass and subsequently generated shock waves further mobilized not only the unstable snow from the surrounding steep slopes of the valley but also the pre-existing debris-covered ice due to a previous mass movement event that occurred between September and October 2016. The impact of a huge rock and ice mass can induce rapid fluidization effect wherein the surrounding material including snow, debris, and boulders start flowing (Huggel et al., 2005). Availability of water along the flow path will further influence the process by easing the fluidization (Dence, 1971). It is also reasonable to assume that the presence of frozen sediments in the Ronti Gad valley from the previous events has further added enough materials to cause hyper-saturated flow the
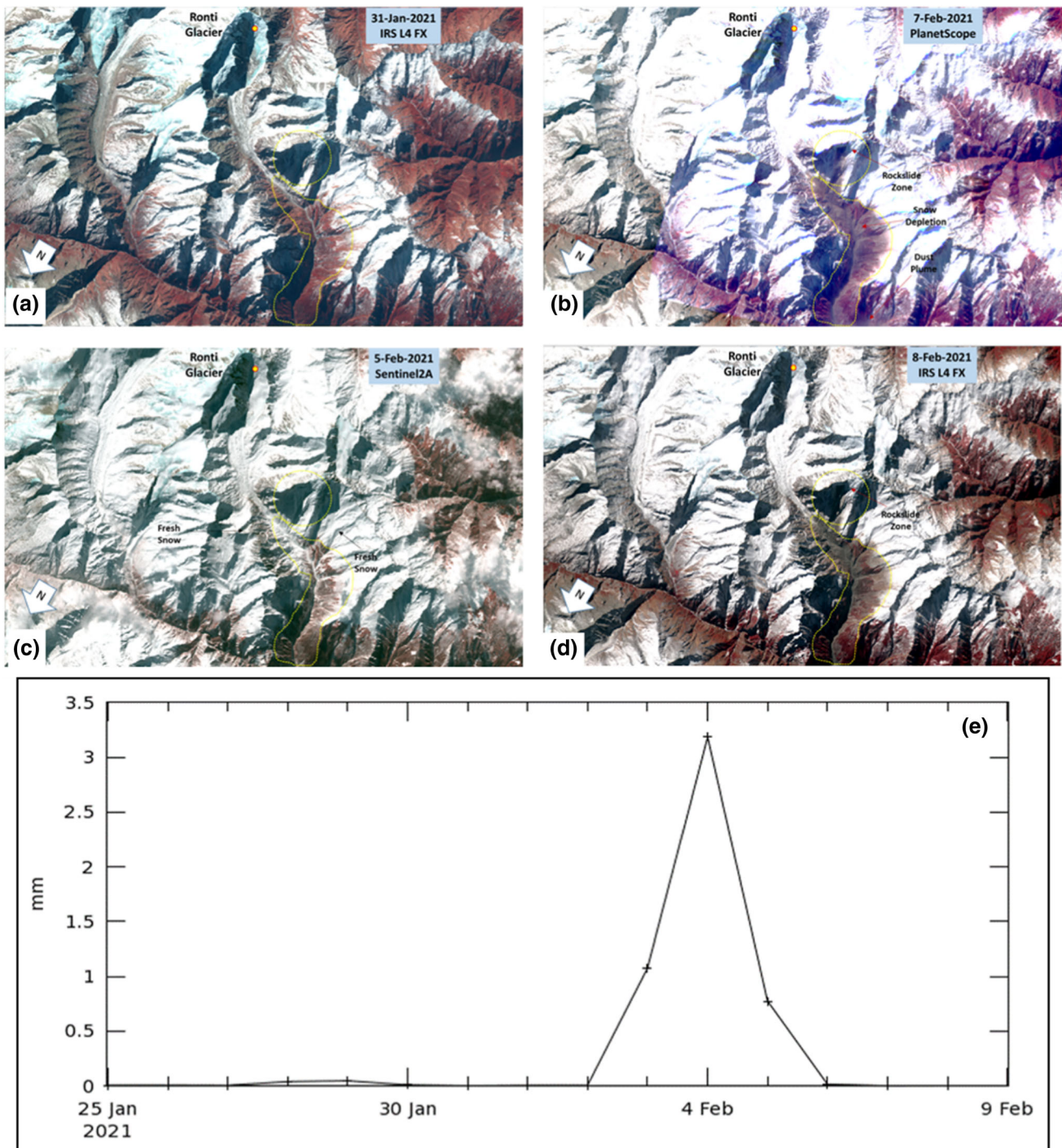
**Fig. 10** **a** & **c**: IRS LISS-IV MX, and Sentinel-2A data showing accumulation of snow in the region prior to the event; **b** & **d** PlanetScope image acquired on the day of the event and IRS LISS IV MX image one day after the event showing depletion in snow cover; **e** :Time series, Area-averaged of daily accumulated precipitation (combined microwave-IR) estimate—Early Run daily 0.1 deg. [GPM GPM_3IMERGDE v06] mm over 2021–01-25—2021–02-08, Region 78.4863E, 29.0039 N, 81.1011E, 31.333 N

downstream. The Rishiganga Hydro Power Project reservoir has also played a major role in facilitating large volume of water from its storage to cause a huge water wave in route to downstream. The debris, mud, boulders carried by the flood water have widened the Ronti Gad valley by washing out the vegetation along its path up to a height of ∼ 100–150 m. The Resourcesat LISS IV satellite images dated October 17, 2019 and February 8, 2021 draped over CARTOSAT-1 DEM clearly show the widening of the Ronti valley owing to the event (Fig. 6b).

This flood finally resulted in extensive loss of human lives, damage to the property and major infrastructures including dams, roads, bridges, houses, etc. Since there was no intense rainfall reported in the higher reaches and no apparent trigger for the flood, people working in the two ongoing construction work of the micro-hydroelectric projects in the Rishiganga and Dhauliganga projects were caught unaware. Based on the sequence of the events and preliminary observations, two probable explanations emerged among the scientists regarding the huge quantum of water released in the event causing the flood and subsequent devastation. The first explanation was based on the assumption that the rockslide was not a single event but occurred in a series, where the initial mass movement might have caused a temporary damming of Ronti meltwater stream and the final mass movement has triggered the outburst from the temporary unstable dam. However, our close aerial survey and the analyses of high-resolution remote sensing images available till now do not provide any conclusive evidence for such damming in the valley. The second and most reasonable inference drawn from our research converges to a possible combination of melting of the ice from the heat produced due to the transformation of kinetic energy and mobilization of snow, ice, debris shock wave generated through the huge impact of the rock and ice and subsequent fluidization in the valley.

## Conclusions

High altitude glaciated mountainous regions of the Himalaya are the source of major river systems in India. Any natural hazards that occur in this terrain will severely impact millions of population inhabited and the infrastructure downstream. While understanding the causative factors of such natural hazards, it is also equally important to recognize the possibilities of such future hazards. The present study carried out on the large-scale mass movement in the Ronti Gad, Rishiganga valley on February 7, 2021 has serious societal concerns. Through the observations of the satellite data as well as aerial survey, it is reasonable to assume that the falling of a huge rock and ice chunk had triggered a mass movement which has caused havoc in the downstream valley. The analysis of seismological data from nearby observatories ruled out the occurrence as an earthquake-triggered rockslide. The remote sensing data and other geospatial technology made a significant contribution in explaining the potential cause of rockslide and the process mechanism, before actually the area could be physically visited. The inputs derived from the satellite remote sensing observations in this investigation have played a critical role in providing inputs for state disaster management agencies for making a decision.

## References

Bhutiyani, M. R., Kale, V. S., & Pawar, N. J. (2010). Climate change and the precipitation variations in the northwestern Himalaya: 1866–2006. *International. Journal of Climatology, 30*, 535–548.

Bhatt, C. M., Rao, G. S., Farooq, M., Manjusree, P., Shukla, A., Sharma, S. V. S. P., Kulkarni, S. S., Begum, A., Bhanumurthy, V., Diwakar, P. G., & Dadhwal, V. K. (2017). Satellite-based assessment of the catastrophic Jhelum floods of September 2014, Jammu & Kashmir, India. *Geomatics, Natural Hazards and Risk, 8*(2), 309–327.

Carrivick, J. L., & Tweed, F. (2016). A global assessment of the societal impact of glacier outburst floods. *Global and Planetary Change, 144*, 1–16. https://doi.org/10.1016/j.gloplacha.2016.07.001.

Champati Ray, P. K., Chattoraj, S. L., Bisht, M. P. S., Kannaujiya, S., Pandey, K., & Goswami, A. (2015). Kedarnath disaster 2013 causes and consequences using remote sensing inputs. *Natural Hazards, 81*, 227–243.

Chow, V. T., Maidment, D. R., & Mays, L. W. (1988). Surface Water. *Applied Hydrology*. (1st ed., pp. 127–166). McGraw-Hill Science.

Dence, M. R. (1971). Impact melts. *Journal of Geophysical Research, 76*, 5552–5565.

Deshmukh, A., Ho, Oh., & E. & Hastak, M. . (2011). Impact of flood damaged critical infrastructure on communities and industries. *Built Environment Project and Asset Management, 1*(2), 156–175.

Dhote, P. R., Thakur, P. K., Aggarwal, S. P., Sharma, V. C., Garg, V., Nikam, B. R., & Chouksey, A. (2018). Experimental Flood Early Warning System in Parts of Beas Basin Using Integration of Weather Forecasting, Hydrological and Hydrodynamic Models. *International Archives of the Photogrammetry, Remote Sensing and Spatial Information Sciences, 5*, 221–225.

Dobhal, D. P., Gupta, A., Mehta, M., & Khandelwal, D. D. (2013). Kedarnath disaster: Facts and plausible causes. *Current Science, 105*(2), 172–173.

Dhote, P. R., Aggarwal, S. P., Thakur, P. K., & Garg, V. (2019). Flood inundation prediction for extreme flood events: a case study of Tirthan River. *North West Himalaya. Himalayan Geology, 402*(128), 140.

Faillettaz, J., Funk, M., & Vincent, C. (2015). Avalanching glacier instabilities: Review on processes and early warning perspectives. *Reviews of Geophysics, 53*(2), 203–224.

Fischer, L., Huggel, C., Kääb, A., & Haeberli, W. (2012). Slope failures and erosion rates on a glacierized high-mountain face under climatic changes. *Earth Surface Processes and Landforms*. https://doi.org/10.1002/esp.3355.

Gruber, S., & Haeberli, W. (2007). Permafrost in steep bedrock slopes and its temperature-related destabilization following climate change. *Journal of Geophysical Research*. https://doi.org/10.1029/2006JF000547,2007.

Guillén Ludeña, S., Cheng, Z., Constantinescu, G., & Franca, M. J. (2017). Hydrodynamics of mountain-river confluences and its relationship to sediment transport. *Journal of Geophysical Research Earth Surface*. https://doi.org/10.1002/2016JF004122.

Hoegh-Guldberg , O , Jacob , D , Bindi , M , Brown , S , Camilloni , I , Diedhiou , A , Djalante , R , Ebi , K , Engelbrecht , F , Guiot , J , Hijioka , Y , Mehrotra , S , Payne , A , Seneviratne , S I , Thomas , A , Warren , R , Zhou , G , Halim , S A , Achlatis , M , Alexander , L V , Allen , M , Berry , P , Boyer , C , Byers , E , Brilli , L , Buckeridge , M , Cheung , W , Craig , M , Ellis , N , Evans , J , Fischer , H , Fraedrich , K , Fuss , S , Ganase , A , Gattuso , J P , Greve , P , Bolaños , T G , Hanasaki , N , Hasegawa , T , Hayes , K , Hirsch , A , Jones , C , Jung , T , Kanninen , M , Krinner , G , Lawrence , D , Lenton , T , Ley , D , Liverman , D , Mahowald , N , McInnes , K , Meissner , K J , Millar , R , Mintenbeck , K , Mitchell , D , Mix , A C , Notz , D , Nurse , L , Okem , A , Olsson , L , Oppenheimer , M , Paz , S , Petersen , J , Petzold , J , Preuschmann , S , Rahman , M F , Rogelj , J , Scheuffele , H , Schleussner , C-F , Scott , D , Séférian , R , Sillmann , J , Singh , C , Slade , R , Stephenson , K , Stephenson , T , Sylla , M B , Tebboth , M , Tschakert , P , Vautard , R , Wartenburger , R , Wehner , M , Weyer , N M , Whyte , F , Yohe , G , Zhang , X & Zougmoré , R B (2018) Impacts of 1.5°C Global Warming on Natural and Human Systems. In: Global Warming of 1.5°C. An IPCC Special Report on the impacts of global warming of 1.5°C above pre-industrial levels and related global greenhouse gas emission pathways, in the context of strengthening the global response to the threat of climate change, sustainable development, and efforts to eradicate poverty [Masson-Delmotte, V., P. Zhai, H.-O. Pörtner, D. Roberts, J. Skea, P.R. Shukla, A. Pirani, W. Moufouma-Okia, C. Péan, R. Pidcock, S. Connors, J.B.R. Matthews, Y. Chen, X. Zhou, M.I. Gomis, E. Lonnoy, T. Maycock, M. Tignor, and T. Waterfield (eds.)]. In Press.

Huggel, C., Zgraggen-Oswald, S., Haeberli, W., Kääb, A., Polkvoj, A., Galushkin, I., & Evans, S. G. (2005). The 2002 ice/rock avalanche at Kolka/Karmadon, Russian caucasus: Assessment of extraordinary avalanche formation and mobility, and application of quickbird satellite imagery. *Natural Hazards and Earth System Sciences, 5*(2), 173–187. https://doi.org/10.5194/nhess-5-173-2005.

Kieffer, S. W., & Simonds, C. H. (1980). The role of volatiles and the lithology in the impact cratering process. *Space Physics, 18*, 143–181.

Kumar, R., Bahuguna, I. M., Ali, S. N., & Singh, R. (2019). *Lake Inventory and evolution of glacial lakes in the Nubra-Shyok basin of Karakoram Range*. . Environment. https://doi.org/10.1007/s41748-019-00129-6.

Martha, T. R., & Kumar, K. V. (2013). September, 2012 landslide events in Okhimath, India—an assessment of landslide consequences using very high resolution satellite data. *Landslides, 10*(4), 469–479.

Negi, H. S., Neha, K., Shekhar, M. S., & Ganju, A. (2018). Recent wintertime climatic variability over the North West Himalayan cryosphere. *Current Science, 114*(4), 25.

Pandey, P., Ali, S. N., Sharma, V., & Champati Ray, P. K. (2020). Focus on Thermokarst Lakes in Indian Himalaya: Inception and implication under warming climate. *Journal of Climate Change, 6*, 59–69. https://doi.org/10.3233/JCC200012.

Pandey, P., Ali, S. N., & Champati Ray, P. K. (2021). Glacier-Glacial Lake Interactions and Glacial Lake development in the Central Himalaya, India (1994–2017). *Journal of Earth Science*. https://doi.org/10.1007/s12583-020-1056-9.

Sattar, A., Goswami, A., & Kulkarni, A. V. (2019). Application of 1D and 2D hydrodynamic modeling to study glacial lake outburst flood (GLOF) and its impact on a hydropower station in Central Himalaya. *Natural Hazards, 97*, 535–553. https://doi.org/10.1007/s11069-019-03657-6.

Shrestha, A., Wake, C. P., Mayewski, P. A., & Dibb, J. E. (1999). Maximum temperature trends in the Himalaya and its vicinity: an analysis based on temperature records from Nepal for the period 1971–94. *Journal of Climate, 12*(9), 2775–2786.

Thakur, P. K., Aggarwal, S., Aggarwal, S. P., & Jain, S. K. (2016). One dimensional hydrodynamic modeling of GLOF and impact on hydropower projects in Dhauliganga River using remote sensing and GIS applications. *Natural Hazards Journal*. https://doi.org/10.1007/s11069-016-2363-4.